Development of a climbing robot for ship hull inspection

Mehdi Shahrami*, Mahdi Khorasanchi

Abstract

Inspection, cleaning, and maintenance of marine equipment, including ships, marine platforms, turbines, and pipelines, have always been of interest to marine industries and oil companies. Over time, fouling by algae and marine organisms on the hull of a ship and marine equipment can cause corrosion and cracks, which must be inspected and then cleaned. Typically, these operations are performed by divers, which has several disadvantages, including the risk of life and an increase in cost and time. Currently, marine robots, including Remotely Operated Vehicles (ROVs) and Autonomous Underwater Vehicles (AUVs), are now expanding and replacing humans to perform reconnaissance missions. In this paper, an inspection robot is designed with the ability to climb the hull of the ship with the help of magnetic tracks. At first, in order to optimally arrange the magnets and obtain the maximum amount of adhesion force, the magnets have been analyzed in ANSYS magnetostatic. Then, the forces entered into the robot from the seawater during the operation were simulated by CFD method. The robot has the main advantages of being compact, lightweight, and simple mechanical structure. It is not only able to climb vertical walls and follows circumferential paths but also able to pass complex obstacles such as bolts, steps, convex and concave corners with almost any inclination regarding gravity. The experiment results show that the climbing robot has a good performance on locomotion and it is successful in negotiating obstacles.

Keywords: Ship inspection**,** Wall-climbing robot, Magnetic tracks, CFD,

Department of Mechanical Engineering, Sharif University of Technology, Tehran, Iran
*__Corresponding author:__ mehdi.shahrami@alum.sharif.edu

1- Introduction

Considering that ships and marine equipment are always in contact with water, algae, and marine biofouling adhere to them, which has negative effects. One of the ways to maintain this equipment is to use antifouling paints, which should be noted that these colors harm marine life (Souto *et al*., 2013). In recent years, we have seen the growth of wall-climbing robots that perform inspection and cleaning operations (Zhengyao *et al.*, 2010). To meet the requirements of underwater ship cleaning, the robot must get close enough to the hull without damaging it. The robot needs six degrees of freedom (DOF) of movement and centimeter position accuracy. The most important functional requirement of the underwater cleaning robot is to maintain continuous absorption capacity due to the steep and irregular surface of the vessel as well as the influence of current, waves, and wind. The adhesion force for a wall-climbing robot depends on the body's material, the surface roughness, and the robot's weight. Adhesion methods include magnetic (Espinoza *et al*., 2015), pneumatic (Brusell et al., 2017), mechanical (Liu *et al*., 2015), electrostatic (Ruffatto *et al*., 2014), and chemical (Sahay *et al*., 2015). Various movement systems are available for these types of robots, including wheeled, legged, tracked, and cable-based systems. However, almost all of these robots use magnetic adhesion, which cannot attach to non-ferromagnetic walls. In addition to the omnidirectional wheel design, steerable wheels are also available for near-omnidirectional movement. Although this robot can be attached to non-ferromagnetic wall surfaces, its motion control is more complicated. In addition, its flexibility is not as good as robots that use omnidirectional wheels (Tavakoli *et al*., 2013).

Tracks are a better alternative to wheels for sticking the robot to the surface. It is possible to install magnets on tracks, which, in addition to strengthening the adhesion between the wheels and the surface, also increases the friction between the robot and the surface, allowing the robot to move safely. Many safety-critical structures in the industry are made of iron materials. Permanent magnet adhesion systems offer advantages such as zero power requirement, high load-carrying capacity, and secure adhesion in case of power failure. A wall-climbing robot called WCCR has been built to inspect the hull of container ships, which uses permanent magnetic wheels for sticking. This robot in order to move between containers is designed with a small shape, and its weight reaches 5.5 kg (Yuanming *et al.*, 2010). The permanent magnet system is designed for another wheeled robot, on which a laser cutting head is installed to separate metal plates (Sattar *et al*., 2016). The head's weight is about 18 kg, which the robot carries in addition to its own weight. Five configurations of Neodymium N42 magnets are designed to produce maximum adhesion force. The size of each magnet is 50*50*12 mm, for this configuration 92 kg of force is obtained. A gap wall-climbing robot usually uses a screw to mount a permanent magnetic attachment device on the side of the wall-climbing robot body close to the work surface. The servo motor rotates the screw to adjust the distance between the permanent magnetic adhesion device and the work surface to obtain sufficient magnetic attraction force. When the external force changes, the dynamic adjustment of the magnetic attraction force can be realized to ensure that the wall-climbing robot is reliably attracted to the work surface and can move flexibly (Zhang *et el*., 2013). The pneumatic adhesion system is widely used for this type of robot, divided into two groups - suction cups (active & passive) and negative pressure thrust. A legged robot has six legs; each leg is equipped with a passive suction cup for

sticking (Kawasaki *et al*., 2014). The movement speed of this robot is low, and it is only able to climb walls on smooth surfaces. The advantages of this system are that it has strong adhesion and does not need an actuator to stick. On the other hand, active suction cups require a vacuum pump to stick. A robot with a track motion system was developed in (Lee *et al*., 2015), which climbs any type of wall regardless of its material. It also can move many loads when moving on the wall. Six suction cups are installed on each track, showing the system's complexity. Mechanical systems use clamping mechanisms or claws for gripping. This system is used for uneven surfaces so that the robot can find the connection points (Bei *et al*., 2016). These robots with mechanical adhesion systems can connect to the surface for a long time without spending energy. Another adhesion method mentioned earlier is the electrostatic method, in which electro-adhesive pads that include conductive electrodes are used (Mao *et al*., 2014). These robots can climb any wall regardless of the wall material. However, they have limited ability to cross obstacles and cannot carry heavy loads. Chemical adhesion method with different movement techniques has been used for wall climbing robots. This adhesion principle can be used with any surface, but adhesion is affected by environmental factors such as temperature, humidity, and dust (Sahay *et al*., 2015). Cleaning methods include rotary brush, water jet, cavitation, ultrasonic, and laser; today, these robots mostly use the water jet cleaning system (changhui *et al*., 2020).

It can be seen from the literature that the wall-climbing robots studied by many researchers only aim at smooth or rough surfaces and rarely prepare wall-climbing robots that adapt to both smooth and rough surfaces. In this article, a robot with permanent magnetic tracks is described, and the evaluation of the robot's movement on the wall is performed.

2- Robot structure

The ship hull inspection robot is designed and built which is depicted in Fig 1. Two servo motors drive this robot. The permanent magnet system has been used to stick this robot, and the magnets are installed on the tracks to increase the friction between the surface and the robot and produce more adhesive force. 80 magnets are placed on the tracks, 32 of which are in contact with the surface. This robot consists of five main parts: the adhesion mechanism, the walking mechanism, the driving mechanism, the frame, and the housing for the placement of electronic parts and the camera. Its dimensions are 680*620*425 (mm3) with a weight of 72 kg, which can move in difficult conditions due to the strong adhesion system. The walking mechanism contains crawlers and sprocket shafts. The locomotion system of this robot consists of two servo motors with a power of 0.4kw geared down with a ratio of 1:50. The power is ultimately transmitted to sprockets each driving a steel traction chains on each side. Guides are designed for the chain rollers to avoid unfavorable deflection of the chain in robot different orientations. The robot could carry a variety of inspection equipment, including cameras, NDT modules, ultrasonic probe, and thickness gauges. In the upper tank-shaped compartment of the robot, cameras and servo drives of ASD B2-042-B type and their power connectors are placed. One of the main tasks of this robot is to show the amount of fouling on the hull to determine if the ship is required to go to the dry dock for cleaning operations.

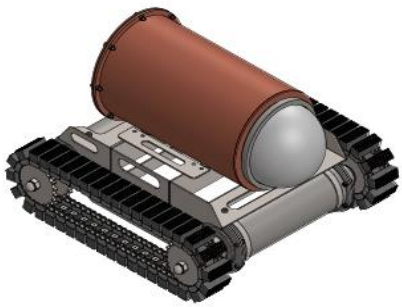

(a)

(b)

Fig 1. (A) Design, (B) Prototype of the ship hull inspection robot

3- Analysis of adhesion requirements

Ship hull has curves and slopes as well the jacket is composed of horizontal and vertical pipes and some inclination ones. When a robot travels on the hull or these pipes, the direction of gravity relative to the robot will change frequently. Moreover, for a robot working in the sea, its stability is also influenced by ocean current and waves. All these factors may cause two types of failures: slipping and falling. To avoid these two failures, the magnetic adhesion units have to provide enough adhesion force.

3-1 Falling analysis

For this robot, it is possible to fall in two modes. First, the robot's adhesion force is less than the external forces imported into the robot, in which case the robot is separated from the surface and falls (Fig 2). The latter is that the amount of torque produced by the adhesion force is insufficient to overcome the robot's external torque, and the robot rotates from the surface and falls (Fig 3).

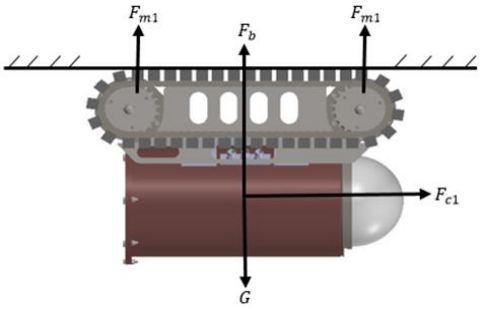

Fig 2. Force analysis of the robot on inverted horizontal surface

According to Fig 2, to prevent the robot from falling, the amount of adhesion required is achieved by equation 1.

$$F_{m1} \geq \frac{1}{2}(G - F_b + \{F_{w1}\}_{max}) \quad (1)$$

For the second case, when the robot is horizontally placed on the body (Fig 3), the minimum amount of adhesion force can be extracted from the following equation.

$$F_{m2} \geq \frac{1}{2l_{m2}}(Gl_g - F_b l_b + \{F_{w2}\}_{max}\, l_{w2}) \quad (2)$$

When the robot is vertically located (Fig 3b), buoyancy, gravity, water force, perpendicular force, and friction force are effective in the fall and slip of the robot. If the robot rotates around point A, but the robot balance is maintained, then:

$$\sum_{i=1}^{n} F_{mi} = \sum_{i=1}^{n} N_i \quad (3)$$

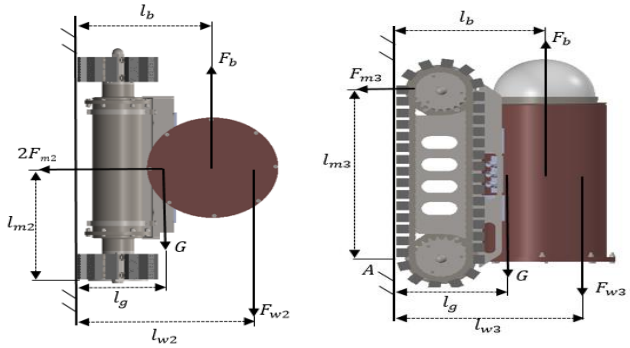

(a) (b)

Fig 3. (a) Robot moves horizontally; (b) vertically

The torque cannot be transmitted around point A because the small rollers are connected to each other. The first top magnet will be separated if the robot rotates around point A. If this point is the support of the rotation, then the simplified equation of torque balance will be as follows: The following relationship can obtain the necessary adhesion force.

$$F_{m3} \geq \frac{1}{2l_{m3}}(Gl_g - F_b l_b + \{F_{w3}\}_{max}\, l_{w3}) \quad (4)$$

3-2 Slipping analysis

Due to the robot's rigidity, if the slip is created, the entire robot will slip and the main reason is insufficient friction. Therefore, when analyzing the robot's slip analysis, the robot can be considered as a particle shown in Fig 4 (Jinchang *et al*., 2018).

$$\{F_m\}_{min} = \frac{1}{\mu}\sqrt{(G - F_b + \{F_w\}_{max})^2 + \{F_c\}^2{}_{max}} \quad (5)$$

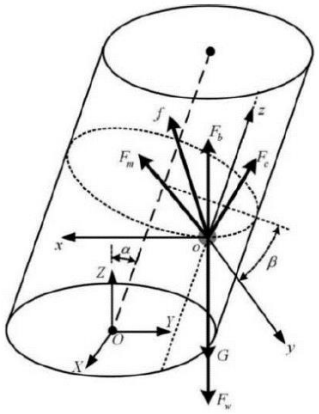

Fig 4. Force analysis of the robot on an inclined pipe

4- Adhesion force

4-1 Magnetic adhesion mechanism

It is known that there is a positive relationship between the adhesive force and dimensions of permanent magnets under the known magnetic material, air gap, and surface thickness. However, as the dimensions of the permanent magnet increase, its weight increases, and meaning that higher adhesive force is needed by the robot to climb on the surface normally. Obviously, there should be a trade-off between the magnetic adhesion system's dimensions, which by which the necessary value of adhesive force and lightweight could be achieved simultaneously. A roller chain, two sprockets, and evenly arranged permanent magnetic units are the parts of each track (see Fig 5). A high-performance magnet with the standard ingredients $Nd_{15}Fe_{77}B_8$ was adopted. The size of the units is 50 × 16 × 16 mm and the weight is 78 g. The adsorption mechanism is using two crawlers with 80 magnets and the number of units in contact with the wall is 36.

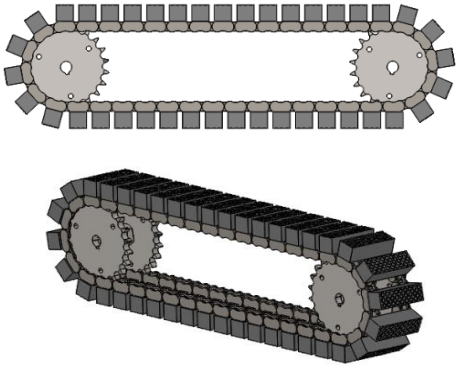

Fig 5. Magnets on the chain

The magnets are connected to a steel plate, to which two screws are welded, and this plate is connected to the chain by nuts. The distance between the center of each magnet and the side magnet is 31.78 mm. The units are coated with polyurethane with a shore hardness of 65 and a density of 0.45 with a thickness of 1.5 mm, which in addition to preventing corrosion, increases the friction force. Fig 6 shows the details of the adhesion system.

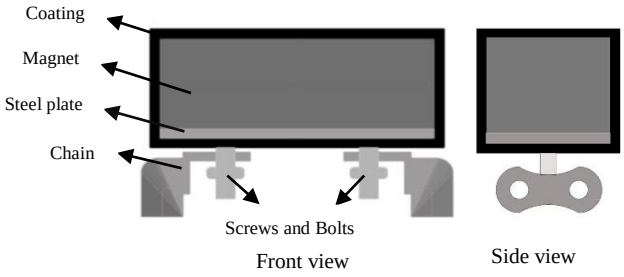

Fig 6. Adhesion mechanism

4-2 Magnetic arrangement

The flow of the magnetic flux in a permanent magnet is from the North Pole to the South Pole which makes a single complete circuit. When several magnets are used, their layout

and magnetizing directions dominate the flux distribution and also the resultant magnetic adhesive force. Obviously, it is necessary to analyze the effect of magnet layout and magnetizing direction on magnetic adhesive to enhance magnetic adhesive force. In designing this system, we can put the magnets together in two ways, and depending on how they are placed, we will decide which structure produces the most adhesion force. In type A, magnets are placed next to each other with similar poles, and in type B, the poles are different.

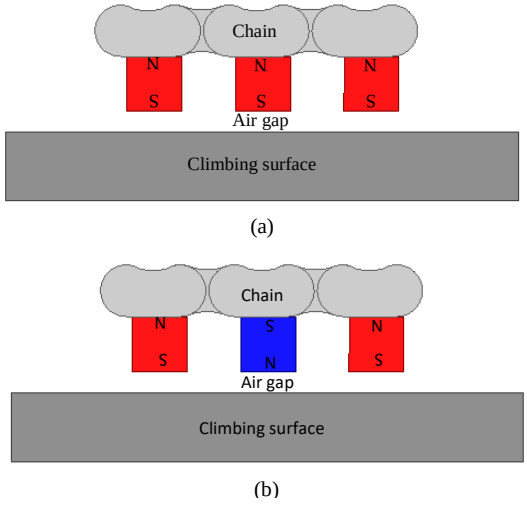

Fig 7: (a) Type A structure, (b) Type B structure

Fig 7 illustrates these two different structures which contain a climbing surface with 20 mm thickness, magnets, and a chain. The air gap is defined as the distance between the climbing surface and the magnet. With increasing the gap, the adhesion force decreases. Including an air gap in all cases is necessary to avoid obstacles and avoid friction.

4-3 ANSYS magnetostatic analysis

The adhesion force of this robot is calculated using finite element magnetic analysis. The design of this system was done in SolidWorks software and then analyzed in ANSYS magnetostatic. In this software, flux density, field strength, magnetic flux, and force simulation can be obtained. Firstly, the magnetic system has meshed, boundary conditions are applied, and then simulation has performed. Here the analysis of the two structures is performed. Fig 8 show the magnetic flux lines of structures A and B. As shown in Fig 8a, flux lines move from the North Pole to the South, producing a certain amount of force. But in Fig 8b, the poles of the center magnet are different, so the direction of the flux lines has changed. In this case, the magnetic flux lines in the middle have a more logical interference with the side magnet lines, which produces more adhesion force. Obviously, higher concentrated flux and a stronger magnetic intensity is attributed to layout B, which is a more desirable layout which is used in the design. It is noteworthy the magnets are attached to the chain from above, but due to the low contact surface of the chain with the magnet, the concentration of the adhesion force is towards the climbing surface.

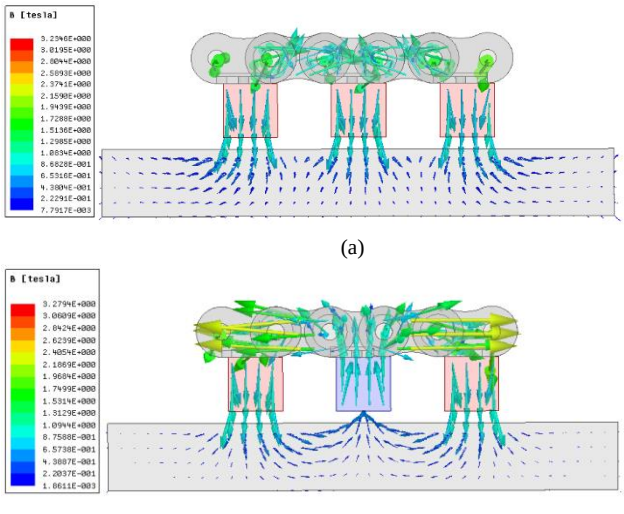

Fig 8: (a) magnetic flux distribution type A, (b) type B

Fig 9 shows the amount of adhesion force at different air gaps. In this figure, there are two curves, the black curve is related to the type A structure and the red curve is related to the type B structure. The maximum amount of adhesion force is in the least air gap, and the

greater the distance, the less adhesion force. Due to the fact that in the type B structure, more adhesion force is produced than in structure A, type B is used for the robot adhesion system.

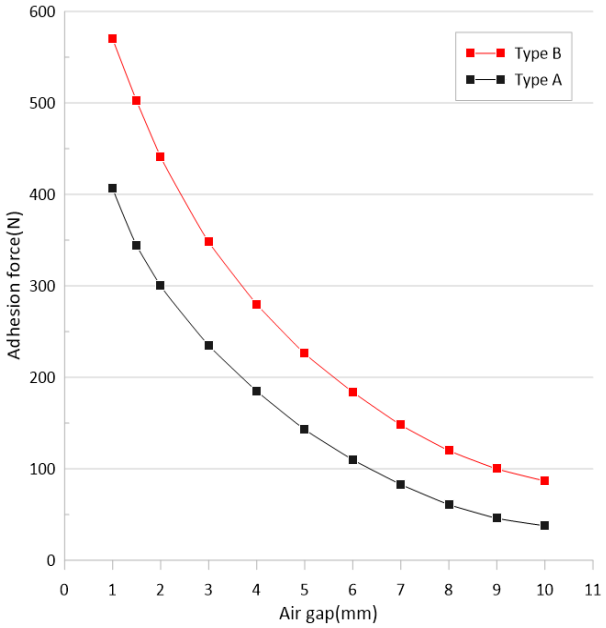

Fig 9: Comparison of two types of structures

4-4 Validation

To confirm the simulation results in ANSYS software, the experimental tests have been performed. In Fig 10, the black curve represents the experimental tests of adhesion force and the red curve represents the selected structure for the system, and by comparing the two curves, it can be said that the error rate is low. For example, at an air distance of 3 mm, the amount of adhesion force in the simulation is 350 N, and in the laboratory test, the value is 325 N Factors influencing this amount of error include the Separation speed of the magnets from the climbing surface and the percentage of system error used for this test.

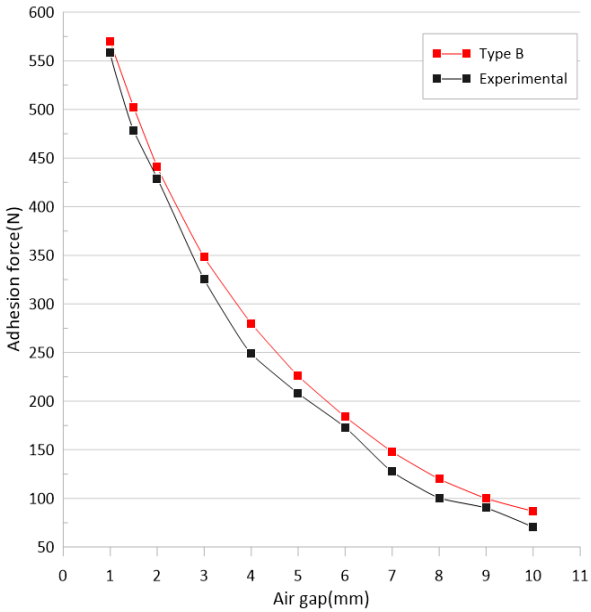

Fig 10: Magnetic forces at different air gaps and experimental results

In this robot 32 magnets are in contact with the wall. The adhesion force must be greater than the minimum force required for the robot to move safely, and also it must be less than the maximum for the motors to ensure that the robot can move. The thickness of the steel hull of ships varies depending on their length, which is between 8 to 20 mm. The amount of air gap can be between 1 to 10 mm depending on the thickness of the foaling. Adhesion force at different air gaps with a wall thickness of 20 mm for 32 magnets is calculated as shown in Table 1.

TABLE I. EFFECT OF AIR GAP ON ADHESION FORCE.

Air Gap(mm)	Adhesion Force(N)
1	6080.271
1.5	5334.642
2	4693.024
3	3733.619
4	2933.302
5	2400.012
6	1814.461
7	1604.644
8	1334.412
9	1067.027
10	854.265

5-Computational fluid dynamics (CFD)

When the robot operates in real conditions and at sea, several forces are effective in moving it. The forces applied to the robot include wave force, water flow force, and in addition, the robot's buoyancy force. In this section, we intend to obtain the amount of forces and torques in three directions x, y, z that impose the robot with the help of Ansys Fluent software, in order to use this force to calculate the minimum adhesion force. Finally, we can find out the maximum distance of the robot from the surface so that its movement is safe. There are three areas on the body of vessels and offshore equipment where the robot may perform inspection and cleaning operations. The first area is the freeboard where the robot moves above the water line. The second area that is the most critical state for the robot and the robot may fall, which is called Splash Zone. In this area, important factors such as the surface's wetness, the robot's sudden force from the sea wave, and the sudden change of the robot's float force can cause the robot to fall. The third area is underwater, where the robot completely dives. In this section, the robot in Splash Zone will be investigated. In these simulations, wave altitude, wavelength, and current speed are 2 m, 10 m, and 0.5 m/s, respectively.

Fig 11: The wave hits the robot

5-1 Robot on wall sided

In this case, the robot is placed horizontally on the wall sided and the flow along the robot hits its front. We have applied the current along the length of the robot because when the current and the wave hit the back or front of the robot, the magnets will separate from the body one by one. But when the flow enters the side of the robot, i.e., in the transverse direction, the amount of wave force and the flow must be much higher than when it hits the back or front of the robot. This is because, in this case, the magnets are arranged transversely together and a sudden force is required to separate the 16 magnets from the body at once. In Fig 11, it can be seen the moment of collision in 2.4 seconds, that at the beginning of the simulation, the robot is out of the water surface, and then a wave with a height of 2 meters hits the robot. This sudden force can be a critical state for the robot. Figs 12(a) and 12(b) show the forces and torques in this situation, respectively.

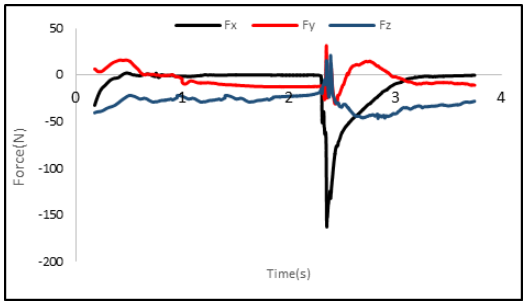

(a)

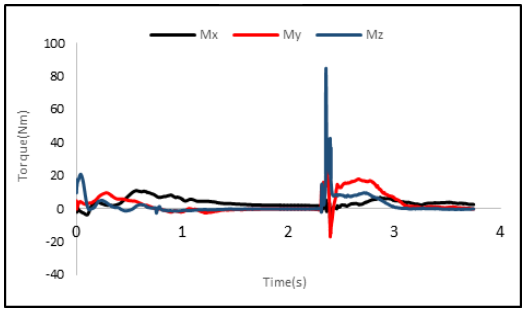

(b)

Fig 12 :(a) force, (b)Torque

The moment the wave hits the robot is 2.4 seconds. Considering that the robot is placed in the direction of the X-axis and the wave hits it, the amount of force is about 150(n). According to equation 2, l_g, l_b, l_{m2} are 0.22, 0.3, and 0.31 meters, respectively. The values of G and $\{F_{w2}\}_{max}$ l_{w2} are 720 newtons and 60(n/m), respectively. By calculating this equation, the minimum force the magnets' top row should have, is 577.5 (n) to prevent rotation and fall. So, the total force of the magnets should be at least 1155(n). Therefore, if the magnets are 9 mm from the surface in this position of the robot, the robot can continue to work. To calculate the value of minimum force of magnets to prevent slipping this value can be easily calculated from the following formula.

$$F_G + F_W - F_B \leq \mu * F_m * 2 \qquad (6)$$

The value of μ is equal to 0.4, and finally, the minimum adhesion force required to prevent slipping is 962.5 (n). Therefore, if the magnets are at a distance of 10 mm from the surface, slipping does not occur.

6- Navigation

Navigation and localization for underwater robots is challenging due to the unavailability of global positioning system (GPS) signals underwater and the complexities and unstable environment of the ocean. Various alternative methods are used for the navigation of these robots, such as the use of inertial navigation system (INS),telemeter, acoustic systems, etc. A significant disadvantage of INS is "drift", which leads to significant error growth with the passage of time in the outputs. In this research, a hybrid navigation system has been investigated and tested, which connects the measurement from INS and the telemeter to reduce drift. In this research, robot position estimation which is a combination of telemeter and INS was presented to reduce the cumulative errors inherent in dead positioning. In order to compensate for the weaknesses in each system, the Kalman filter was designed. Fig 13 shows the proposed system.

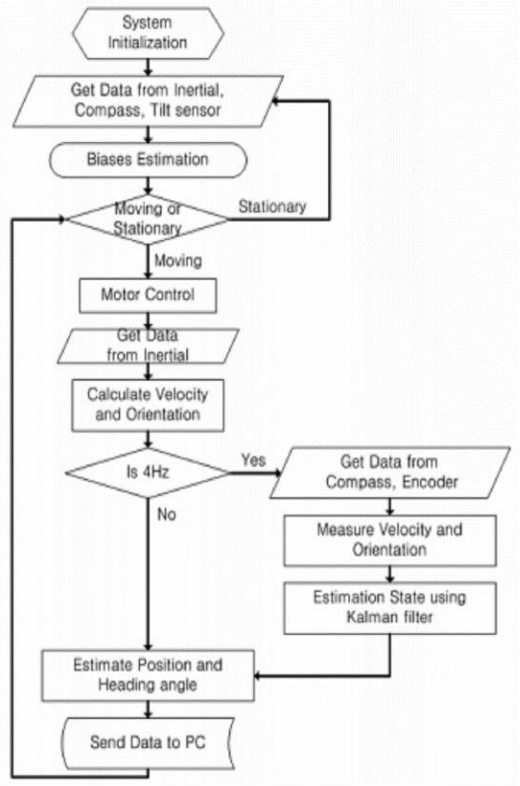

Fig 13: Navigation system flowchart

7- Vision system

The vision framework comprises of a Wi-Fi HD 1080 p camera. The camera is installed in the most ideal position on the robot; this is to ensure that the operator is able to see clearly the condition of the hull in-front of the robot shown in Fig 14. With the real-time feedback from the camera, robot can be controlled precisely. The camera operates at 5 V, with a power rating of three watts. A gimbal is used to prevent the camera from shaking in critical situations.

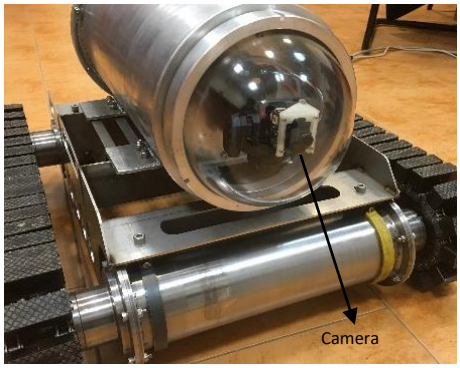

Fig 14: Vision system

8- Control system

The control system of the climbing robot which controls its movements and navigates it along a predetermined trajectory is a very significant part. It has the following characteristics:

- Reliable, convenient and flexible to operate.
- In real time the moving directions and moving speed can be adjusted.
- A wired remote control is applied.

Due to the harsh working environment, the control mode is limited and here, a wired remote control mode is chosen via which the multiple moving speed can be set by pressing different functional keys. This mode allows the robot to be controlled by an operator on the work field without any delay; it can also be controlled by the industrial computer via communication system. The control system of the climbing robot is based on hierarchical control architecture (Schoeneich *et al*., 2011). It includes the host computer and guest computer as suggest. The aim of the control hierarchy is to relieve the robot operator from arduous low-level control through converting a series of high-level tasks into a sequence of driving signals. The main function of the guest computer system is to receive and process the orders from the host computer and then output the analog voltage signals to control servo drivers which further control the rotation of the servo motor and the inspection instruments so as to control robot motions (Haocai *et al*., 2017). The configuration of the control system of the wall-climbing robot is illustrated in fig 15.

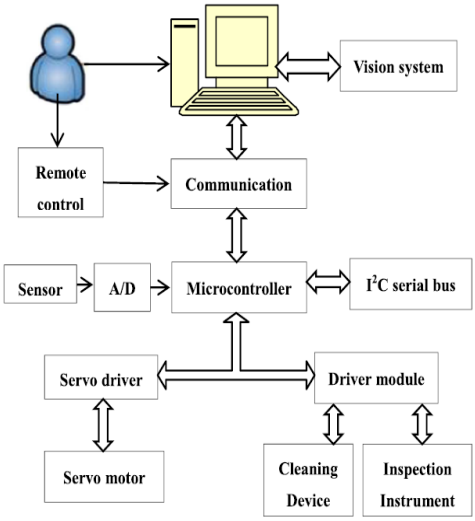

Fig 15: Configuration of the control system of the robot

9- Motion performance test

The robot for inspection operation needs to have adsorption stability and good motion performance. We conducted robot movement tests under different situations to verify its stability and accurate motion capabilities (fig 16). When the climbing robot with the detection instruments conducts inspection work, it may fail to complete the missions and even slides down or overturns in extreme cases, if its payload is overloaded or the operation parameters are not properly set. To verify the performance and validate the parameters of the robot, a series of experimental tests were conducted in sea conditions (fig17). The tests include climbing speed testing, payload capacity testing, and obstacle-overcoming performance testing. The robot has a wide range of speed which mainly depends on the frequency of motor. The maximum speed is even over 0.5 m/s. The robot prototype was controlled to climb both vertically and horizontally with decent speed.

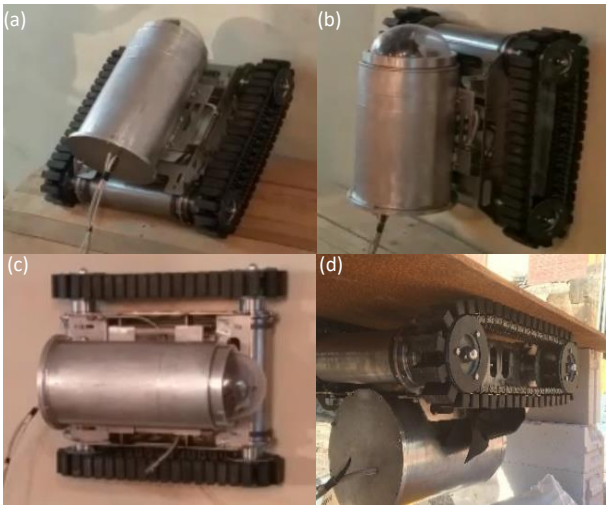

Fig 16: Robot prototype experiment in laboratory: (a) transitioning moment, (b) climbing motion after transitioning on vertical surface, (c) horizontal orientation, and (d) upside down on horizontal surface.

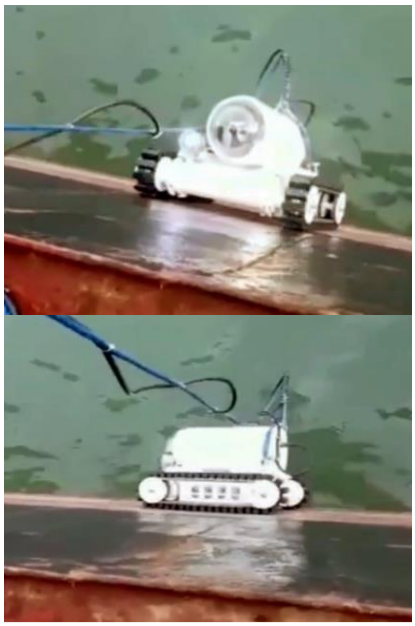

Fig 17: Robot operation in on the ship hull

10- Conclusion

The underwater robot in this paper is developed to replace divers that wipe off marine lives on ship hull and steel pipes, such as jackets of offshore oil platforms. Status of falling and slipping are analyzed to determine the adhesion requirements. Optimization is conducted to achieve the best structure parameters of the combined magnet adhesion unit. The optimization is conducted in two steps to effectively save time, and its conditions are simplified by an established approximation method.

The adhesion system was designed and the most optimal structure was selected. CFD analysis was performed and it was determined that when the robot is in the splash zone, according to the wave force, at what distance from the surface it can perform the operation and not fall. Finally, prototype is manufactured and the experiments are taken in the Shipyard. The prototype experiments show that the robot driving system works in a good condition. It was amply able to meet the design requirements with respect to payload capability, surface adaptability, and maneuverability, all of which were validated by the locomotion tests.

11- Acknowledgements

The work was financially supported by the head of the "Applied ocean research group" of the Sharif University of Technology. The authors would like to thank Sharif University in Iran for providing laboratory space. The valuable technical support from the staff and students throughout the project is also appreciated. The authors are grateful to reviewers for their valuable comments, which improved the readability of this paper significantly.

References

Brusell, A., Andrikopoulos, G., and Nikolakopoulos, G., 2017. "*Novel considerations on the negative pressure adhesion of electric ducted fans: An experimental study*" in Proc 25th Mediterranean Conference on Control and Automation (MED), 2017, pp. 1404-1409.

Bei,W. Fengyu,X. and Zhong,Y., 2016. "*Grasping mechanism and prototype experiment of bionic sharp hook on rough surface*" in Proc. 2016 23rd International Conference on Mechatronics and Machine Vision in Practice (M2VIP), 2016, pp. 1-6.

Changhui,L. Weicheng, C., 2020. "*Review of Underwater Ship Hull Cleaning Technologies*" Journal of Marine Science and Application, pp.1-15.

Souto, D., Faiña, A., López-Peña, F. and Duro, R.J., 2013. "*Lappa: a new type of robot for underwater non-magnetic and complex hull cleaning*", IEEE International Conference on Robotics and Automation (ICRA), Karlsruhe, 6-10 May, pp. 3409-3414.

Zhengyao, Y., Yongjun, G., Zuwen, W., Xingru, W. and Zengmeng, Z., 2010. "*Large wall climbing robots for boarding ship rust removal cleaner*", Robot, Vol. 32 No. 4, pp. 560-567.

R. V. Espinoza, A. S. de Oliveira, L. Valéria, R. de Arruda, and F. N. Junior., 2015. "*Navigation's stabilization system of a magnetic adherence-based climbing robot*" *Journal of Intelligent & Robotic Systems*, vol. 78, p. 65.

Liu, Y., Sun, S., Wu, X and Mei,T., 2015. "*A wheeled wall-climbing robot with bio-inspired spine mechanisms*" Journal of Bionic Engineering, vol. 12, pp. 17-28.

Lee,G. Kim,H. Seo, J. Kim, H.and Kim,S., 2015. "*MultiTrack: A multi-linked track robot with suction adhesion for climbing and transition*" Robotics and Autonomous Systems, vol. 72, pp. 207-216.

Ruffatto,D., Parness.,A and Spenko,.M ., 2014. "*Improving controllable adhesion on both rough and smooth surfaces with a hybrid electrostatic/gecko-like adhesive*" Journal of The Royal Society Interface, vol. 11, p. 20-31.

Sahay.,R , Low.,H, Baji,.A, Foong.,S and K. L. Wood,. 2015. "*A state-of-the-art review and analysis on the design of dry adhesion materials for applications such as climbing micro-robots*" Rsc Advances, vol. 5, pp. 50821-50832.

Sattar, P. Hilton, and Howlader,M ,. 2016. "*Deployment of laser cutting head with wall climbing robot for nuclear decommissioning*" ," Proc. of the 5th World Conf. On Marine Engineering, Rome, pp. 135-142.

Schoeneich, P., Rochat, F., Nguyen, O.T.D., Moser, R., Mondada, F., 2011. TRIPILLAR: a miniature magnetic caterpillar climbing robot with plane transition ability. Robotica 29 (7), 1075–1081.

Haocai, H. Danhua, L. Zhao, X ., 2017. "*Design and performance analysis of a tracked wall-climbing robot for ship inspection in shipbuilding"* Ocean Engineering, pp. 224-230.

Tavakoli, M.; Viegas, C.; Marques, L. OmniClimbers., 2013. "*Omni-directional magnetic wheeled climbing robots for inspection of ferromagnetic structures*". Robot. Auton. Sys, 61, 997–1007.

Yuanming, Z., Tony, D., Kias, A., 2010. "*Design and Optimization of Magnetic Wheel for Wall and Ceiling Climbing Robot*" Proceedings of the 2010 IEEE International Conference on Mechatronics and Automation August 4-7, 2010, Xi'an, China.

Jinchang, F. Canjun, Y. Yanhu, C. Hansong, W and Zhengming, H., 2018. "*An underwater robot with self-adaption mechanism for cleaning steel pipes with variable diameters*" Industrial Robot:An International Journal, Vol. 45 Issue: 2, pp.193-205.

Kawasaki, S and Kikuchi,K., 2014. "*Development of a small legged wall climbing robot with passive suction cups*" in Proc. The 3rd International Conference on Design Engineering and Science–ICDES, pp. 112-16.

Mao,J. Qin,L. Wang,Y. Liu,J. and Xue,L., 2014. "*Modeling and simulation of electrostatic attraction force for climbing robots on the conductive wall material*" in IEEE International Conference on Proc. Mechatronics and Automation (ICMA), pp. 987-992.

Wu, M.; Pan, G.; Zhang, T.; Chen, S.; Zhuang, F.; Yan-Zheng, Z., 2013. "*Design and optimal research of a non-contact adjustable magnetic adhesion mechanism for a wall-climbing welding robot*". Int. J. Adv. Robot. Syst, 10, 63.